VIROLOGY

Cytomegalovirus US28 regulates cellular EphA2 to maintain viral latency

Amanda B. Wass[1,2]†, Benjamin A. Krishna[1,2]†‡, Laura E. Herring[3,4], Thomas S. K. Gilbert[4], Masatoshi Nukui[1,2]§, Ian J. Groves[1,2,5], Abigail L. Dooley[1,2,5], Katherine H. Kulp[1,2], Stephen M. Matthews[1,2], Daniel M. Rotroff[6,7], Lee M. Graves[4], Christine M. O'Connor[1,2,5]*

Cytomegalovirus (CMV) reactivation from latency following immune dysregulation remains a serious risk for patients, often causing substantial morbidity and mortality. Here, we demonstrate the CMV-encoded G protein–coupled receptor, US28, in coordination with cellular Ephrin receptor A2, attenuates mitogen-activated protein kinase signaling, thereby limiting viral replication in latently infected primary monocytes. Furthermore, treatment of latently infected primary monocytes with dasatinib, a Food and Drug Association–approved kinase inhibitor used to treat a subset of leukemias, results in CMV reactivation. These ex vivo data correlate with our retrospective analyses of the Explorys electronic health record database, where we find dasatinib treatment is associated with a significant risk of CMV-associated disease (odds ratio 1.58, $P = 0.0004$). Collectively, our findings elucidate a signaling pathway that plays a central role in the balance between CMV latency and reactivation and identifies a common therapeutic cancer treatment that elevates the risk of CMV-associated disease.

INTRODUCTION

Human cytomegalovirus (CMV) establishes persistent, lifelong infections, supported by latency, wherein the viral genome is maintained, with limited production of infectious virus. Undifferentiated hematopoietic progenitor and circulating myeloid cells support latent infection, and reactivation from latency occurs under specific conditions associated with immunosuppression, cellular differentiation, and inflammation (*1*). While mostly asymptomatic in healthy individuals, CMV infections are a major clinical threat to the immunocompromised, immunonaïve, and immunosuppressed, including an increasing number of organ transplant recipients (*2*). Reactivation during times of immunosuppression leads to widespread viral dissemination, often causing severe morbidity and mortality. In addition to immune suppression, it is also possible that certain therapeutic interventions unintentionally foster an environment favoring CMV reactivation. Thus, understanding the latent and reactivation phases of infection at a molecular level may inform treatment. For example, leukemia patients treated with dasatinib, a tyrosine kinase inhibitor, following hematopoietic stem cell transplant (HSCT) have a significant increase in CMV reactivation. The mechanism by which this occurs is unknown, although the cellular targets of dasatinib, including Src and the membrane-bound receptor tyrosine kinase (RTK) Ephrin receptor A2 (EphA2), may provide clues. Both of these host proteins modulate mitogen-activated protein kinase (MAPK) signaling; activated Src up-regulates MAPK kinase (MEK)/extracellular signal–regulated kinase (ERK) via Ras/Raf activation (*3*), and conversely, EphA2 forward signaling attenuates ERK1/2 activity (*4*). As a result, EphA2 regulates a variety of cellular processes including integrin-mediated adhesion, proliferation, and development (*5*). Presumably, dasatinib-mediated Src and EphA2 inhibition would thus lead to activation of MEK/ERK signaling, thus representing an additional mechanism by which these host proteins regulate CMV reactivation.

One of four CMV-encoded G protein–coupled receptors (GPCRs), US28 is a potent signaling molecule, expressed during both lytic and latent infection. We and others previously identified the requirement for US28 in both the establishment and maintenance of latency (*6*–*14*). US28's functions during latency are multifaceted, including monocyte reprogramming (*14*), disruption of DNA sensing pathways (*7*), and modulation of host factors that regulate the major immediate early (MIE) enhancer/promoter locus, whose repression is critical for latency (*15*). US28 promotes association of repressive factors at the MIE locus, such as heterochromatin protein-1 (*11*) and CCCTC-binding factor (*6*), yet attenuates proactivation factors, such as activator protein-1 (AP-1) via down-regulation of the AP-1 subunit, c-Fos (*10*). This is a critical step in silencing the MIE enhancer/promoter, as recruitment of AP-1 to this locus leads to its activation and subsequent viral reactivation (*16*). While the mechanism(s) underlying US28-mediated AP-1 attenuation remain outstanding, MEK/ERK signaling regulates downstream c-Fos. Thus, as a cell surface signaling protein, it is possible US28, in conjunction with EphA2, results in attenuated MEK/ERK–c-Fos signaling, thereby supporting a cellular environment favoring viral latency.

Here, we show that US28 attenuates the Src-MEK/ERK–c-Fos signaling axis in coordination with EphA2. Using parallel, unbiased mass spectrometry (MS)–based proteomics, we find US28 up-regulates and interacts with EphA2, ultimately resulting in diminished activity of Src, MEK, ERK, and c-Fos, each of which we show must be attenuated to maintain viral latency. Furthermore, pharmacological inhibition of this pathway in wild type (WT)–infected cells prevents viral reactivation, despite stimulation with cytokines

[1]Department of Genomic Medicine, Lerner Research Institute, Cleveland Clinic, Cleveland, OH 44195, USA. [2]Infection Biology Program, Global Center for Pathogen and Human Health Research, Lerner Research Institute, Cleveland Clinic, Cleveland, OH 44195, USA. [3]UNC Proteomics Core Facility, University of North Carolina at Chapel Hill, Chapel Hill, NC 27599, USA. [4]Department of Pharmacology, University of North Carolina at Chapel Hill, Chapel Hill, NC 27599, USA. [5]Molecular Medicine, Cleveland Clinic Lerner College of Medicine of Case Western Reserve University, Cleveland Clinic, Cleveland, OH 44195, USA. [6]Department of Quantitative Health Sciences, Lerner Research Institute, Cleveland Clinic, Cleveland, OH 44195, USA. [7]Endocrinology and Metabolism Institute, Cleveland Clinic, Cleveland, OH 44195, USA.
*Corresponding author. Email: oconnoc6@ccf.org
†These authors contributed equally to this work.
‡Present address: Cambridge Institute of Therapeutic Immunology and Infectious Disease, Department of Medicine, University of Cambridge School of Clinical Medicine, Cambridge CB2 0QQ, UK.
§Deceased.

that trigger CMV reactivation. Genetic knockdown or pharmacological inhibition of EphA2 with dasatinib results in up-regulation of active forms of Src and MEK/ERK in monocytic cells. In line with this, dasatinib treatment of infected primary CD14$^+$ cells results in CMV reactivation even in the absence of external reactivation stimuli. This is consistent with our retrospective analysis of the Explorys de-identified electronic health record (EHR) clinical database that reveals a correlation between dasatinib treatment and CMV-associated disease. Collectively, our findings elucidate a signaling pathway that plays a central role in the balance between CMV latency and reactivation and identifies an increase in the odds for CMV reactivation in an at-risk population.

RESULTS

US28 modulates Src-MEK/ERK activity during CMV latent infection

Our previous findings revealed US28-mediated signaling promotes CMV latency by suppressing c-Fos at both the transcriptional and posttranslational levels during latent infection, thereby preventing the AP-1 transcription factor complex from binding and activating the MIE enhancer/promoter (*10*). Since MAPK signaling activates c-Fos (*17*), we hypothesized that US28 signaling attenuates the MAPK pathway to ultimately reduce activated c-Fos. To test this, we used THP-1 monocytic cells to stably express wild type US28 (*10*) or two US28 signaling mutants, US28-R129A or US28-ΔN, each under the control of a doxycycline (DOX)–inducible promoter. The R129A mutation in the "DRY" motif renders US28 incapable of coupling G proteins and, thus, is considered a signaling deficient mutant (*18*). US28-ΔN lacks amino acids 2 to 16, resulting in a US28 mutant unable to bind several of its known ligands (*18*), thus allowing us to assess the requirement for ligand engagement. Using these cell lines, we evaluated phosphorylated and total forms of proteins in the MAPK-Fos pathway. We also evaluated Src, a cellular kinase that regulates MEK/ERK signaling upstream and plays a role in CMV reactivation in dendritic cells (*19*). US28 expression attenuates MEK1/2 and ERK1/2 activity (Fig. 1A), the latter of which is consistent with previous data in the same cells expressing constitutively expressed US28 (*11*). Also in response to US28 expression, Src Tyr^{416} phosphorylation is diminished, while Src Tyr^{527} phosphorylation is increased (Fig. 1A), indicative of inactive Src (*3*). In accordance with our previous findings (*10*), both phospho- and total-c-Fos are reduced following WT US28 expression. While DOX treatment alone increases both active and total forms of c-Fos (*10*, *20*, *21*), robust expression of US28 impairs this up-regulation (Fig. 1A). Expression of each of the two signaling mutants, as indicated by the FLAG epitope tag, does not modulate the activity of Src, MEK1/2, ERK1/2, or Fos when compared to wild type US28 (Fig. 1A). We also confirmed the inhibition of this pathway in the context of CMV infection by assessing the activity of ERK as a downstream effector in the MAPK pathway. TB40/E*mCherry* (WT)–infected CD14$^+$ cells display an increase in phospho-ERK relative to mock-infected cultures (Fig. 1B), consistent with previous reports in CD34$^+$ hematopoietic progenitor cells (HPCs) (*19*). However, infection with a virus in which we deleted the entire *US28* open reading frame (ORF), TB40/E*mCherry*-US28Δ (US28Δ) (*22*), results in further augmentation of ERK phosphorylation when compared to WT-infected CD14$^+$ cells. This finding highlights the fact that signaling is not binary, and intermediate activity of signaling proteins has measurable effects on the host cell

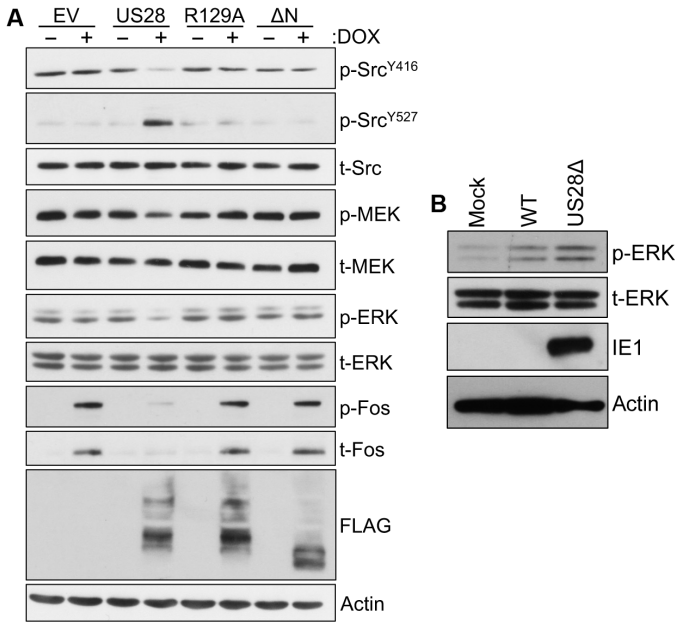

Fig. 1. US28 attenuates the Src-MAPK-Fos signaling pathway in a ligand- and G protein–dependent manner. Phosphorylated (p) and total (t) forms of the indicated proteins were assessed by immunoblot. (**A**) THP-1 cells transduced with pSLIK empty vector control (EV), pSLIK-US28-3xF (US28), pSLIK-US28-R129A-3xF (R129A), or pSLIK-US28-ΔN-3xF (ΔN) were treated for 24 hours with vehicle (−DOX) or DOX (+DOX). (**B**) CD14$^+$ cells were infected with WT or US28Δ (MOI = 1.0 $TCID_{50}$ per cell) and sorted by FACS at 1 dpi for mCherry expression. Parallel mock-infected cultures were sorted for the total live cell population as a control. Cells were cultured under latent conditions and harvested 7 dpi. IE1 is shown as a marker of lytic infection. (A and B) Representative blots shown; $n = 3$ biological replicates.

environment. In this case, the increase in phospho-ERK we observe in US28Δ-infected cells is concomitant with an infection that instead favors lytic replication, as indicated by immediate early 1 (IE1) expression, a CMV-encoded immediate early protein highly expressed during lytic, but not latent, infection (Fig. 1B). Collectively, these findings suggest that US28-mediated attenuation of Src-MEK/ERK–c-Fos signaling requires both its ligand binding domain and G protein–coupling motif.

Our above data reveal US28 down-regulates MAPK signaling in hematopoietic cells, and since we and others have shown a requirement for US28 in maintaining latency (*7*, *8*, *10*–*14*), we hypothesized that US28 regulates the MAPK pathway to aid in maintaining viral latent infection in CD14$^+$ monocytes. To this end, we infected primary CD14$^+$ cells with either WT or US28Δ under latent conditions (latency media), then treated cells from each infection with targeted inhibitors of ERK1/2 (SCH772984; 125 nM), MEK (selumetinib; 0.5 μM), or Src (PP2; 10 μM) (fig. S1, A to F). We maintained these cultures in medium that supports latency (latency media) or conditions that favor reactivation (reactivation media) and measured the frequency of infectious centers by extreme limiting dilution analysis (ELDA), the gold standard for ex vivo CMV latency studies. Consistent with previous findings (*7*, *8*, *10*–*14*), US28Δ-infected cells fail to maintain viral latency (Fig. 2 and fig. S1G). However, the addition of each inhibitor resulted in a significant reduction in infectious center frequencies in the US28Δ infections, to levels similar to those observed for WT latently infected cells. In addition, the presence of the targeted inhibitors significantly impaired viral reactivation from

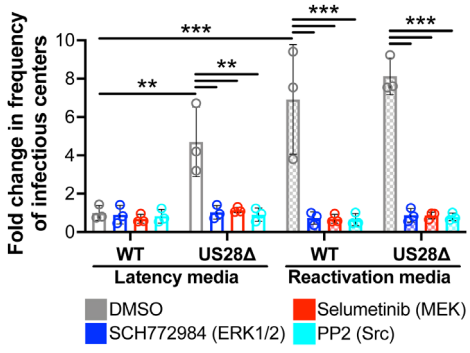

Fig. 2. Pharmacological inhibition of Src-MEK/ERK suppresses reactivation in WT-infected CD14$^+$ cells. CD14$^+$ cells were infected (MOI = 1.0 $TCID_{50}$ per cell) with WT or US28Δ for 7 days and then treated with the indicated compounds (see also fig. S1, A to F) under conditions that favor latency (latency media, open bars) or reactivation (reactivation media, checked bars). The frequency of infectious centers was evaluated, and data are plotted as fold change in frequency of infectious centers relative to latent, WT-infected cells (open gray bar). Each data point (circles) denotes the mean of three technical replicates (see fig. S1G). Error bars indicate the SD of three biological replicates. Statistical significance was calculated by two-way analysis of variance (ANOVA) with Tukey's test for multiple comparisons. $^{**}P < 0.01$, $^{***}P < 0.001$.

latency for both WT and US28Δ infections (Fig. 2 and fig. S1G). Together, these results suggest US28 attenuates the Src-MAPK signaling axis during latency, whose activation is critical for CMV reactivation.

US28 up-regulates and interacts with cellular EphA2 during latent infection

To define the underlying mechanism by which US28 modulates MAPK signaling during latency, we used two unbiased approaches to (i) profile kinome changes in response to US28 expression and (ii) define US28 interacting partners that could influence its function(s). First, we evaluated changes in the cellular kinome in response to US28 expression in THP-1 monocytic cells compared to control cells using multiplexed kinase inhibitor beads coupled with MS (MIBS-MS) to quantitatively measure kinase expression and abundance (*23*, *24*). Overall, we quantified 174 kinases, and we found that US28 significantly dysregulates 59 kinases at 2 hours and 85 kinases at 6 hours after DOX treatment (Fig. 3, A and B, and data S1). Notably, we observed a reduction in multiple MAPK pathway components, including significant attenuation of MEK family members, including MEK2, as well as ERK1 and ERK2. MEK1 abundance was also reduced, but the levels of inhibition did not meet our stringent cutoff criteria for significance (data S1). US28 expression also resulted in a significant increase in EphA2 (Fig. 3, A and B, and data S1), whose forward signaling results in attenuation of MAPK activity (*4*, *25*, *26*). EphA2 is also a target of dasatinib, a second-line therapeutic administered to patients with Philadelphia chromosome–positive (Ph$^+$) acute lymphoblastic leukemia (ALL) and chronic myeloid leukemia (CML). In a small retrospective study of patients with Ph$^+$ ALL and CML after allogeneic HSCT, dasatinib treatment correlated with increased CMV reactivation (*27*). Given these data and the coincident down-regulation of MAPK pathway proteins we observed in our dataset, we focused on EphA2 as a potential contributor to this process. Latent infection of primary CD14$^+$ cells with WT virus induced EphA2 expression and phosphorylation as early as 2 days post infection (dpi), which, although diminished, remained elevated through 7 dpi (Fig. 3C). In contrast, CD14$^+$ cells infected with US28Δ virus displayed significantly reduced EphA2 expression and activity through 7 dpi (Fig. 3C), consistent with the timing of phospho-ERK up-regulation (Fig. 1B). These data suggest US28 up-regulates EphA2 during latent infection.

In addition to up-regulating and activating EphA2, we also found that US28 physically interacts with this cellular protein. We leveraged proximity labeling technology (*28*), whereby we inserted the biotin ligase gene, *birA*, conjugated to a C-terminal hemagglutinin (HA) epitope tag in-frame with the *US28* ORF to generate TB40/E-*mCherry*-US28-bioID-HA (US28-bioID-HA; fig. S2). We then infected fibroblasts with US28-bioID-HA, added biotin 18 hours before harvesting the cells at 48 hours post-infection (hpi), and analyzed the biotin-conjugated proteins following streptavidin capture by affinity purification-MS (AP-MS). After eliminating proteins designated as likely contaminants based on comparison to the CRAPome (*29*), our analysis revealed a total of 261 proteins, of which 224 cellular and 9 viral proteins, including EphA2, were statistically significant (Fig. 3D and data S2). Since we also identified EphA2 in our kinome analysis, we focused on this RTK as a potential US28 binding partner and confirmed the US28:EphA2 interaction in the context of both lytic and latent infection. To this end, we used a viral recombinant; three tandem FLAG epitopes were inserted in-frame at the US28 C terminus, TB40/E*mCherry*-US28-3xF (US28-3xF) (*22*), to infect primary fibroblasts (lytic) or primary CD14$^+$ monocytes (latent). In the context of lytic (Fig. 3E) and latent (Fig. 3F) infection, we confirmed EphA2 interacts with US28 by coimmunoprecipitation (co-IP). Collectively, these data demonstrate US28 up-regulates and interacts with cellular EphA2.

EphA2 represses Src-MEK/ERK-Fos signaling in monocytic cells

We next confirmed that EphA2 attenuates MAPK signaling in cells that support CMV latency using genetic and pharmacological approaches in parallel. EphA2 knockdown in THP-1 cells (Fig. 4A and fig. S4A) displayed a significant up-regulation of activated forms of Src (Tyr^{416}) and ERK, as well as active and total c-Fos, compared to control cells (Fig. 4A), suggesting that EphA2 regulates this pathway, consistent with previous findings in nonhematopoietic cell types (*4*). This is similar to our observations in THP-1 cells that express the US28 signaling mutants, US28-R129A or US28ΔN (Fig. 1A). While THP-1 cells are an accepted model system for some aspects of CMV latency, a major drawback of these cells is their inefficient support of viral reactivation (*30*). Thus, as a surrogate for latency and reactivation, we evaluated *UL123* transcription, as this viral gene is significantly repressed during latent infection, yet robustly expressed from the MIE locus during lytic replication [e.g., (*10*, *11*, *30*)]. While EphA2 knockdown had no impact on viral lytic replication (fig. S5), knockdown in THP-1 cells correlated with a significant up-regulation of *UL123* expression compared to control THP-1 cells (fig. S4B), suggesting that reduced EphA2 expression fails to repress MIE-driven lytic gene transcription during WT latent infection. Collectively, these data suggest EphA2 expression aids in the repression of the Src-MAPK-c-Fos signaling axis to maintain the repression of lytic gene expression.

Dasatinib induces CMV reactivation

While our data suggest that EphA2 activity functions in maintaining viral latency, the THP-1 model system limits our ability to effectively

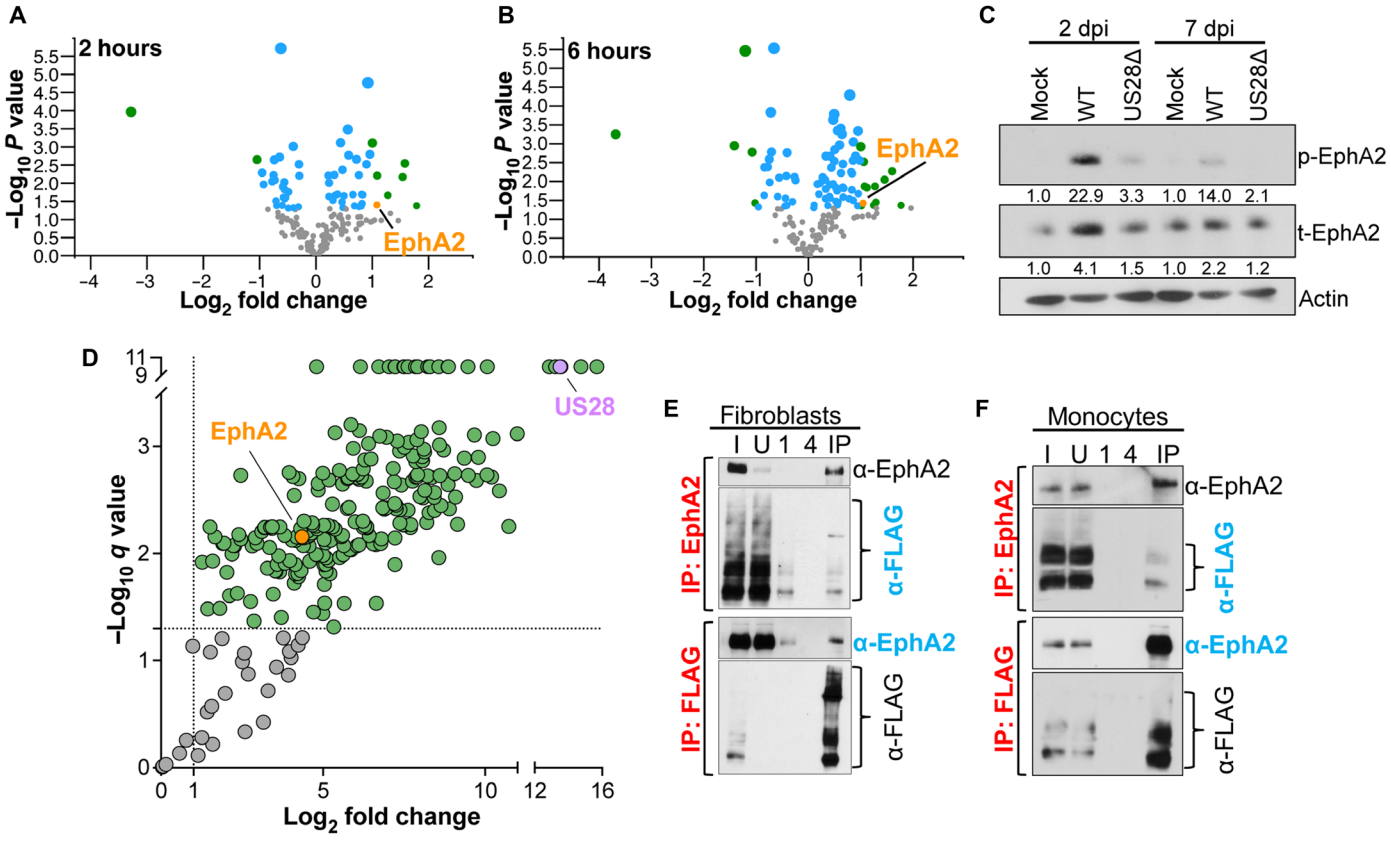

Fig. 3. US28 interacts with EphA2 and increases its protein levels. (**A** and **B**) pSLIK empty vector (EV) control or pSLIK-US28 (US28)–expressing THP-1 cells were treated +DOX for (**A**) 2 hours or (**B**) 6 hours. MIB-MS was used to analyze the global kinome in response to US28 expression (data S1). Ratios (pSLIK-US28/pSLIK-control) were calculated by dividing LFQ intensities of each kinase and then $\log_2$-transformed. Identified kinases are shown as data points: blue, $P < 0.05$; green, $P < 0.05$ and $\log_2$ fold change >1 or <−1; orange, EphA2 ($P < 0.05$ and $\log_2$ fold change >1). Data point size correlates to degree of significance, where the larger data points are more statistically significant. (**C**) $CD14^+$ monocytes were mock-, WT-, or US28Δ-infected (MOI = 1.0 $TCID_{50}$ per cell) under latent conditions for 2 or 7 days, then assessed for phosphorylated (p-) and total (t-) EphA2; expression of each was quantified by densitometry relative to actin (values noted below each blot). (**D**) AP-MS/MS data of NuFF-1 cells infected with TB40/E*mCherry*-US28-BirA-HA (MOI = 1.0 $TCID_{50}$ per cell; see also fig. S2) at 48 hpi. Green data points, FDR-corrected $q < 0.05$ ($-\log_{10} > 1.3$, denoted by the dashed line); gray data points, not significant; orange data point, EphA2; purple data point, US28 (each $q < 0.05$; $-\log_{10} > 1.3$). See also data S2. (**E** and **F**) IP-Western of (E) NuFF-1 cells lytically infected with TB40/E*mCherry*-US28-3xF (US28-3xF; MOI = 1.0 $TCID_{50}$ per cell, 2 dpi) or (F) $CD14^+$ monocytes latently infected with US28-3xF (MOI = 1.0 $TCID_{50}$ per cell, 7 dpi). (E and F) I, input; U, unbound; 1, wash no. 1; 4, wash no. 4; IP, immunoprecipitated sample. Top: IP, EphA2 (red label); Western blot, FLAG (blue label). Bottom: IP, FLAG (red label); Western blot, EphA2 (blue label). IgG control IPs are shown in fig. S3. (A, B, and D) $n = 2$ biological replicates; (C, E, and F) representative blots shown; $n = 3$ biological replicates.

evaluate viral reactivation. Thus, we used a second approach to assess EphA2's impact on MAPK signaling in primary cells. To this end, we used the pharmacological inhibitor, dasatinib, which targets specific kinases, including EphA2 and Src, in turn leading to downstream EphA2-mediated MAPK activity in CML and AML cells in culture (*31*, *32*). Dasatinib treatment is implicated in reactivation of CMV following HSCT (*27*). Treatment of primary $CD14^+$ cells with dasatinib resulted in an increase in active forms of both Src (e.g., Src^{Y416}) and ERK (Fig. 4B and fig. S6A). Phosphorylation of Src^{Y527}, which is associated with an inhibitory form of this protein, remains unchanged in dasatinib-treated primary $CD14^+$ cells (Fig. 4B). To further evaluate the contribution of EphA2 activity to MAPK signaling during CMV latency, we assessed latency and reactivation in primary cells. Dasatinib treatment of WT latently infected $CD14^+$ cells for 24 hours resulted in an increase in ERK and Fos activity (Fig. 5, A and B) and an increase in IE1 expression (Fig. 5B). This correlated with a significant increase in infectious center frequency, similar to levels we observe in WT-infected cells cultured in reactivation medium without dasatinib treatment (Fig. 5C and fig. S6B). Patients receiving a daily dasatinib dose of 100 mg result in an average plasma exposure of 813.5 nM/hour, based on the area under the plasma drug concentration time curve (AUC) of 397 ng/ml per hour indicated in the drug package insert. Thus, the concentration we used (0.5 μM), which results in CMV reactivation ex vivo, is below the exposure level observed for patients receiving the recommended starting dosage for adults. These findings suggest that treatment of latently infected $CD14^+$ cells with dasatinib results in MAPK activation and positively influences CMV reactivation from latency.

Last, to determine the association between dasatinib treatment and CMV reactivation during natural infection, we performed a retrospective cohort analysis of U.S.–based health care systems participating in the Explorys database. To this end, we assessed de-identified, aggregated EHRs by searching for patient medication with the term, "dasatinib," which yielded 3230 patient records, a significant increase

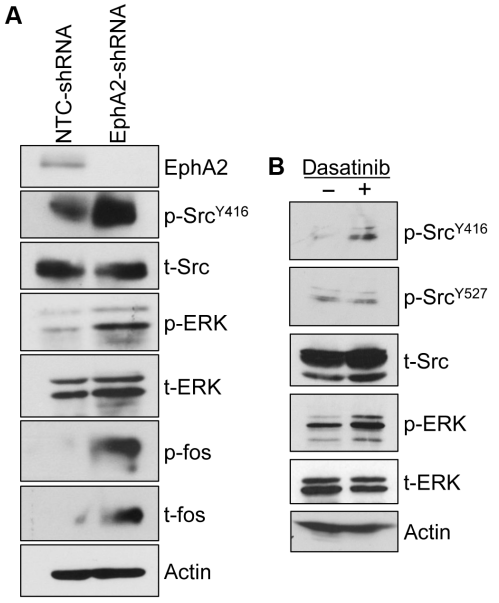

Fig. 4. EphA2 regulates Src-ERK-Fos activity in monocytic cells. Immunoblot of the indicated proteins (p, phosphorylated; t, total). (**A**) Nontargeted control (NTC) shRNA or EphA2 shRNA#1 stably transduced THP-1 cells. (**B**) Primary CD14$^+$ cells treated with dasatinib (0.5 μM) or vehicle (DMSO, – dasatinib) for 24 hours. (A and B) Representative blots are shown; $n = 3$ biological replicates.

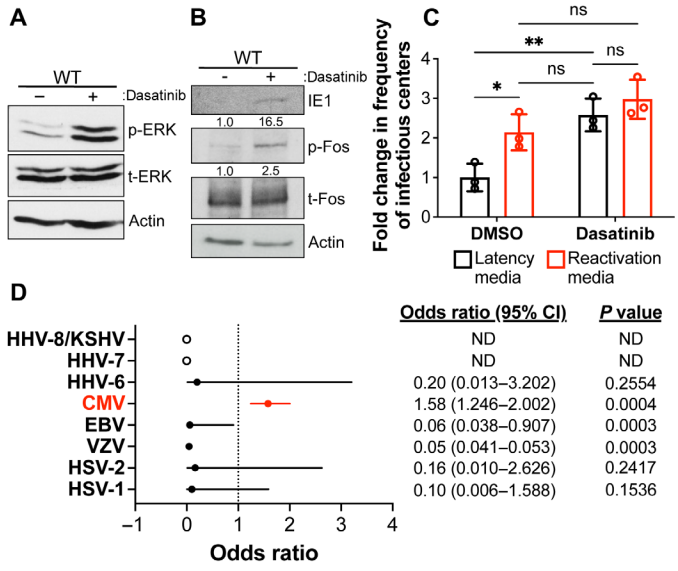

Fig. 5. Dasatinib induces CMV reactivation in latently infected cells and correlates with greater risk for CMV-associated disease. (**A** to **C**) CD14$^+$ cells were infected with TB40/*EmCherry* (WT; MOI = 1.0 $TCID_{50}$ per cell) under latent conditions for 7 days. Immunoblot of (A) phospho- and total-ERK or (B) IE1, phospho-, and total-Fos after treatment with dasatinib (0.5 μM) or vehicle (DMSO; – dasatinib) for 24 hours. (B) Expression of IE1 was quantified relative to actin. Expression of phospho-Fos was quantified by densitometry relative to total-Fos first, then actin. Values are noted below each blot. (A and B) Representative blots shown; $n = 3$ biological replicates. (C) At 7 dpi, infected cells were either maintained in media promoting latency (latency media, black bars) or cultured in cytokine-rich media to promote reactivation (reactivation media, red bars) in the presence of either DMSO or dasatinib (0.5 μM, see also fig. S6A). The frequency of infectious centers was quantified by ELDA. Each data point (circles) denotes the mean of three technical replicates (fig. S6B). Error bars indicate the SD of three biological replicates. Statistical significance was calculated by two-way ANOVA with Tukey's test for multiple comparisons. *$P < 0.048$, **$P = 0.009$, ns = not significant. (**D**) The Explorys EHR database was used to perform a retrospective analysis on viral disease outcome for patients treated with dasatinib. ORs and 95% CIs were determined by Fisher's exact test. Statistical tests were adjusted for multiple testing using the Benjamini-Hochberg FDR approach (*85*), and FDR $P < 0.05$ was used as a threshold for significance (shown on the right). ND, not determined.

over a prior study that targeted a small (n = 21) subset of Ph$^+$ ALL and CML HSCT patients receiving this treatment (*27*). These records were then cross-referenced by diagnoses of "viral disease" and/or "infection" by searching against those patients diagnosed with each human herpesvirus (HHV) (Fig. 5D and tables S1 and S2). Consistent with previous findings (*27*), patients treated with dasatinib demonstrated a significantly higher risk for CMV-associated disease [odds ratio (OR), 1.58; 95% confidence interval (CI), 1.246 to 2.002; false discovery rate (FDR) P value = 0.0004] when compared to disease outcomes associated with each of the other HHVs (Fig. 5D and tables S1 and S2). These data also suggest that dasatinib treatment results in reduced risk of disease due to Epstein-Barr virus (EBV: OR, 0.06; 95% CI, 0.038 to 0.907; FDR, P value = 0.0003) or varicella zoster virus (VZV: OR, 0.05; 95% CI, 0.041 to 0.053; FDR, P value = 0.0003; Fig. 5D). While there were not enough patient data to evaluate a possible correlation between dasatinib and disease due to HHV-7 or HHV-8/Kaposi's sarcoma–associated herpesvirus (KSHV), we found no correlation between treatment with this inhibitor and HHV-6, herpes simplex virus-1 (HSV-1), or HSV-2 (Fig. 5D and tables S1 and S2). Collectively, these findings suggest that compared to other HHVs, dasatinib treatment poses a unique risk for CMV reactivation and disease during natural infection.

DISCUSSION

Here, we identified a previously unknown mechanism by which CMV US28 maintains latency. During latent infection of monocytic cells, US28 interacts with EphA2, thereby attenuating Src-MAPK-Fos activity. Pharmacological inhibition of EphA2 with dasatinib or genetic disruption of this host RTK activates Src-MAPK-Fos signaling and promotes viral reactivation, which is phenotypically similar to infection with a US28 deletion virus. Consistent with these molecular findings, a retrospective analysis of patient data in the Explorys Database reveals that CMV-associated disease is significantly increased over other herpesvirus-associated maladies in patients treated with dasatinib. Collectively, our data point to a mechanism by which US28 regulates the cellular RTK, EphA2, to coordinate Src-MAPK–c-Fos down-regulation, thereby securing viral latency.

A number of viruses use Eph receptors and their respective ephrin ligands and/or Eph-ephrin signaling to promote infection (*33*). EphA2, in particular, is an entry receptor for the gammaherpesviruses, EBV and KSHV, via viral gH/gL heterodimers that complex with EphA2's ligand binding domain (*33*–*36*). This could explain why dasatinib treatment has lower odds of association with disease due to EBV (Fig. 5D). While EphA2 as a receptor for CMV has not been directly assessed, this cellular RTK is significantly up-regulated following CMV lytic infection of fibroblasts (*23*). However, EphA2 knockdown in fibroblasts had no impact on cell-free or cell-associated virus production (fig. S5), suggesting that a reduction in this protein does not affect viral entry. It is possible, however, low EphA2 levels that remain in our knockdown fibroblast cells are sufficient to allow for CMV entry, warranting further interrogation. Nonetheless, while

EphA2 appears to function differently in the context of gammaherpesviral infections, our findings indicate this RTK is important for CMV latency.

How does CMV or, more specifically, US28, regulate EphA2? Our data reveal that US28 not only up-regulates EphA2 but also physically interacts with this cellular RTK. Similar to EBV and KSHV gH/gL, perhaps US28 binds EphA2 upon virion attachment, thereby triggering its activation. US28 is incorporated into the mature viral particle and is expressed immediately upon infection of hematopoietic cells, which aids in the establishment of latency (*8*, *10*). While CMV may not use EphA2 as a cellular receptor for binding/entry, US28's interaction with EphA2 could occur as early as virion attachment to the host cell membrane, triggering signaling events that favor latency. Alternatively, perhaps US28 and EphA2 oligomerize, in turn altering their signaling properties in an independent and/or collective fashion. Such physical interactions between RTKs and GPCRs are not without precedent [e.g., (*37*)]. In addition, bidirectional transactivation between GPCRs and RTKs is also well established. Adaptor proteins, such as Src, impart cross-talk between these receptor families (*38*), which could further explain a role for Src in our data. G proteins and β-arrestins certainly regulate GPCR signaling, but emerging data suggest that they can affect RTK activity as well (*39*). Future work aimed at these biochemical and molecular details will undoubtedly strengthen our understanding of the mechanisms underpinning EphA2 regulation during CMV infection, in addition to the cross-talk between this cellular RTK and the viral GPCR, US28.

US28's engagement of EphA2 to thereby regulate signaling and ultimately repress the MIE enhancer/promoter is likely specific to cells that support latent infection. US28 is dispensable for efficient IE1/2 expression (*22*, *40*, *41*) and viral replication (*12*, *14*, *22*, *42*–*44*) in a variety of cells that support lytic infection. These findings suggest that US28 functions in a cell type– and perhaps infection type–specific manner. Such specificity likely also applies to the cellular factors CMV regulates, as EphA2, like US28, is important for latency, yet is not required for lytic infection (fig. S5). US28, as with other latently expressed CMV-encoded proteins, is also expressed during lytic infection. Understanding how US28 switches from potentiating pro-latency signaling to that which favors reactivation and lytic infection is of great interest and a focus of our ongoing work in this area. Undoubtedly, understanding such nuances will inform key steps in the latent-to-lytic switch and provide insight into the host-pathogen relationship across cell types critical for CMV pathogenesis.

Our retrospective analysis of the Explorys EHR database indicates that the relative odds of CMV reactivation following dasatinib treatment are significantly increased, supported not only by our mechanistic studies in vitro but by others' published work. Approved since 2006, dasatinib is used to treat Ph^+ CML in chronic phase or as a second-line therapeutic for patients with Ph^+ CML or Ph^+ ALL who no longer tolerate or respond to other treatments, such as imatinib and nilotinib. Investigators noted the possibility for herpesvirus reactivation following dasatinib treatment soon after it was approved for clinical use (*45*). In addition to the work from Prestes and colleagues highlighted above (*27*), studies from other groups revealed that patients with chronic phase CML treated with dasatinib developed CMV-induced hemorrhagic colitis (*46*–*48*). Other reports of CMV-associated disease in patients treated with dasatinib have been published, including CMV colitis in patients with chronic CML and acute ALL (*49*) and patients with Ph^+ ALL after HSCT (*50*), as well as CMV hepatitis in a pediatric patient with CML (*51*). Of note, however, these prior studies are either case reports, often only including data from a single patient, or detailed findings from a small cohort of patients who received dasatinib [e.g., 21 of 109 total patients, (*27*)]. This led to the speculation that CMV reactivation was not necessarily due to dasatinib itself but rather the impact on immune suppression. Several groups have reported that dasatinib treatment suppresses natural killer (NK) and T cell functions [e.g., (*52*–*57*)]. Large granular lymphocytes (LGLs), morphologically distinct yet phenotypically heterogeneous lymphocytes composed of NK and/or T cells, are expanded with dasatinib treatment and are associated with favorable clinical outcomes (*58*–*60*), indicating an interesting paradox between dasatinib-induced immunosuppression and dasatinib-induced LGL expansion. Despite enhanced therapeutic response in some leukemic patients, in a small cohort study of 25 dasatinib-treated patients with ALL and CML, Kreutzman and colleagues (*61*) found that dasatinib-induced LGL expansion correlated with CMV reactivation. These data are in contrast to a separate analysis in a similar-sized cohort, in which the authors concluded that CMV reactivation was uncommon despite LGL expansion. However, only 2 of 25 patients were CMV immunoglobulin G positive (IgG^+) (*62*) versus 15 in the earlier study (*61*), which could account for differences in reactivation numbers. It is certainly possible that the mechanism by which dasatinib induces reactivation is a combination of immune dysregulation coupled with the coordinated attenuation of MAPK signaling by US28 and EphA2. Furthermore, dasatinib also targets the non-RTK, ABL1, which is also up-regulated following US28 expression (data S1). ABL1's function during CMV reactivation is unknown, although treatment of lytically infected fibroblasts with imatinib impairs CMV replication (*63*). Understanding this kinase in the context of CMV latency and reactivation, especially in the context of Ph^+ ALL or CML, is the aim of future work. In addition, it is important to point out that while our data show that the relative increase in CMV reactivation in patients is significantly increased with dasatinib treatment, it is clear that not all individuals receiving this drug will suffer from complications due to CMV. This suggests other biological and epidemiological variables may contribute to CMV reactivation in a subset of patients receiving dasatinib. Nonetheless, our findings, coupled with other reports in the literature, suggest patients undergoing dasatinib treatment should be monitored closely for CMV reactivation and disease.

As a therapeutic approved for use in cancer patients, much of the molecular characterization of dasatinib has been performed using cancer cell lines. From work from multiple groups, it is evident that dasatinib's impact on cell signaling is tissue and cell type specific (*26*, *31*, *64*–*68*). For example, in breast cancer (*66*, *67*) and uterine cancer (*68*) cell lines, dasatinib-mediated EphA2 inhibition results in a reduction of phospho-ERK. Conversely, dasatinib inhibits active EphA2 and phospho-Src at Tyr^{527} (the inhibitory phospho site), concomitant with a slight increase in activated ERK in papillary thyroid carcinoma–derived cell lines (*65*). In the HL60 cell line, which was established from an AML patient, dasatinib induces cellular differentiation and increased MAPK activity, as measured by phospho-MEK and ERK (*31*). This is in accordance with our data using myeloid cells herein, as well as those published by Packer *et al.* (*32*), who showed dasatinib activated MEK and ERK in multiple cell lines tested. Collectively, these findings across various cell types derived from different tissues suggest that the impact dasatinib has on host cell signaling downstream of EphA2 and Src is complicated and influenced by other context-specific factors.

Similarly, CMV's impact on host cell signaling and protein activity may also be cell type specific. While our data reveal that MAPK activity is attenuated during latency yet required for reactivation in $CD14^+$ monocytes, Buehler *et al.* (*69*) showed that pharmacological inhibition of MEK with binimetinib or ERK1/2 using SCH772984, the latter of which we used herein, facilitates CMV reactivation in $CD34^+$ HPCs. While $CD34^+$ HPCs and $CD14^+$ monocytes both harbor CMV latently, these cells have distinct phenotypes; thus, it is not surprising to find subtle differences such as these. Our data, in fact, align with others' that showed MAPK signaling promoted CMV reactivation in monocyte-derived dendritic cells (*19*). Ex vivo growth conditions, cell type, and/or tissue type specificity may indeed explain other differences, including the finding that US28 expression is required for reactivation, but not latency, in fetal liver–derived $CD34^+$ cells (*70*). Collectively, these findings highlight the complexity of the relationship between CMV and host cells, further elucidating that such cell type–specific nuances will undoubtedly better our understanding of this host-pathogen relationship and the factors required to maintain (and reactivate) latent virus. Our findings reveal a previously unknown means by which CMV regulates cellular signaling to maintain viral latency and provides an underlying biological mechanism as to how dasatinib enhances CMV reactivation.

MATERIALS AND METHODS

Reagents

All antibodies, cell lines, and tools used herein are described in full in table S3.

Cells

Newborn human foreskin fibroblasts (NuFF-1, passages 13 to 25; GlobalStem) were maintained in Dulbecco's modified Eagle's medium (DMEM), supplemented with 10% fetal bovine serum (FBS), 2 mM L-glutamine, 0.1 mM nonessential amino acids, 10 mM Hepes, and 100 U/ml each of penicillin and streptomycin. 293T cells [American Type Culture Collection (ATCC)] were maintained in DMEM, supplemented with 10% newborn calf serum (NCS), and 100 U/ml each of penicillin and streptomycin. THP-1 cells (ATCC) were maintained in RPMI 1640 supplemented with 10% FBS and 100 U/ml each of penicillin and streptomycin at a density between 3×10^5 and 8×10^5 cells/ml. Primary $CD14^+$ monocytes were isolated from de-identified cord blood samples (Abraham J. & Phyllis Katz Cord Blood Foundation d.b.a. Cleveland Cord Blood Center and Volunteer Donating Communities in Cleveland and Atlanta) by magnetic-activated cell separation (described below) and maintained in X-VIVO15 media (XVIVO-15; Lonza) with 100 U/ml each of penicillin and streptomycin at 7.5×10^5 cells/ml. All cells were maintained at 37°C and 5% CO_2.

Viruses

The bacterial artificial chromosome (BAC)–derived clinical CMV strain TB40/E (clone 4) previously engineered to express mCherry to monitor infection, TB40/E*mCherry* (*71*), was used in this study, referred to throughout as WT virus. TB40/E*mCherry*-US28-3xF and TB40/E*mCherry*-US28Δ are described elsewhere (*22*). TB40/E*mCherry* was used as a template to generate a recombinant virus expressing US28 with C-terminal birA-HA using galactokinase (galK) recombineering, as described in detail elsewhere (*72*). Briefly, the *galK* gene was amplified from pGalK (*72*) by polymerase chain reaction (PCR) using primers listed in table S4. Recombination-competent SW105 *Escherichia coli* (*72*) containing TB40/E*mCherry* were transformed with the resulting PCR product. The gene for biotin ligase, *birA*, with a C-terminal HA epitope tag, was amplified from plasmid pcDNA3.1 MCS-BirA(R118G)-HA, which was a gift from K. Roux [Addgene plasmid no. 36047; http://n2t.net/addgene:36047; research resource identifiers (RRID):Addgene_36047; (*28*)], using the primers listed in table S4. GalK-positive clones were electroporated with the PCR product, and mutants were then counter-selected against galK. TB40/E*mCherry*-US28-birA-HA was verified for genomic accuracy by Sanger sequencing using the primers in table S4. All viral stocks were propagated on NuFF-1 cells and titered by 50% tissue culture infectious dose ($TCID_{50}$) on naïve NuFF-1 cells.

Generation of lentivirally transduced cells

The lentivirus-transduced THP-1 cell lines, THP-1-pSLIK-hygro and THP-1-pSLIK-US28-3xF, were described previously (*10*). pSLIK-US28-R129A-3xF and pSLIK-US28-ΔN-3xF vectors were generated by gateway cloning, detailed elsewhere (*73*). In brief, US28-R129A-3xF and US28-ΔN-3xF DNA fragments were PCR-amplified using TB40/E*mCherry*-US28-R129A-3xF and TB40/E*mCherry*-US28-ΔN-3xF, respectively, as templates. These recombinant BACs were previously published (*10*). The primers, which include 5′ Spe I and 3′ Xba I restriction enzyme sites, are shown in table S4. DNA fragments were purified using the GFX PCR DNA and Gel Band Purification Kit (Millipore Sigma), according to the manufacturer's instructions. The resulting fragments and the pEN_TmiRc3 entry vector [a gift from I. Fraser, Addgene plasmid no. 25748, (*74*)] were digested with Spe I and Xba I [New England Biolabs (NEB)], after which the entry vector was dephosphorylated using calf intestinal phosphatase (NEB). Following gel purification of the DNA, the insert fragments were ligated with the entry vector using T4 ligase (NEB). After confirming ligation, the insert-containing entry vector was used for gateway recombination with the destination vector pSLIK-hygro [a gift from I. Fraser, Addgene plasmid no. 25737; (*74*)], using the Gateway LR Clonase Enzyme Mix (Thermo Fisher Scientific), according to the manufacturer's protocol. The resulting pSLIK-US28-R129A-3xF and pSLIK-US28-ΔN-3xF lentiviral constructs were confirmed by Sanger sequencing, using primers listed in table S4.

To generate transduced cell lines, 293T cells were first cotransfected with pCMV-VSV-G envelope [a gift from B. Weinberg; Addgene plasmid no. 8454, (*75*)] and pCMV-ΔR8.2 (a gift from D. Trono; Addgene plasmid no. 12263) packaging plasmid, along with either pSLIK-hygro, pSLIK-US28-R129A-3xF, pSLIK-US28-ΔN-3xF, or EphA2 shRNA and control plasmids (table S3) at a ratio of 3:5:10, using Fugene 6 Transfection Reagent (Promega; pSLIK THP-1 cell lines) or Lipofectamine 2000 (Thermo Fisher Scientific; EphA2 knockdown and control lines), following the manufacturers' protocols. Media were collected 48 and 72 hours after transfection, clarified through a 0.45-μm filter, and concentrated by ultracentrifugation (82,200*g*, 4°C, 90 min), after which the viral pellet was resuspended in X-VIVO15 (Lonza) for transduction of THP-1 cells or DMEM for transduction of NuFF-1 cells. The concentrated lentiviruses were then used to transduce 1×10^6 THP-1 cells by centrifugal enhancement (1000*g*, 30 min, room temperature) or 1×10^6 NuFF-1 cells, each in the presence of polybrene (4 μg/ml). All cells were returned to culture overnight at 37°C/5% CO_2. The following day, THP-1 cells were clarified by centrifugation (35 min, 450*g*, room temperature, without the brake) onto Ficoll Paque Plus (Millipore Sigma), washed

three times in 1× phosphate-buffered saline (PBS), and returned to culture in fresh RPMI 1640–based media, as described above. NuFF-1 cells were washed three times with 1× PBS and replenished with DMEM, supplemented as indicated above. THP-1 cells transduced with the pSLIK vectors were selected using hygromycin B (500 μg/ml; Millipore Sigma). For the EphA2 knockdown and control lines, transduced cells were selected with puromycin (Thermo Fisher Scientific); 1.5 μg/ml was used for THP-1 cells, and 700 ng/ml was used for NuFF-1 cells. When necessary, cell debris was removed from the THP-1 cell cultures by cushioning cells onto Ficoll Paque Plus (Millipore Sigma), as above. Knockdown of EphA2 protein expression was assessed by immunoblot (described below); US28-R129A-3xF and US28-ΔN-3xF protein expression was similarly assessed following treatment with DOX (1.0 μg/ml) or vehicle [dimethyl sulfoxide (DMSO)] for 24 hours in the newly generated, respective THP-1 lines.

Latency and reactivation assays

Primary $CD14^+$ cells were isolated from cord blood using human CD14 MicroBeads (Miltenyi Biotec) followed by magnetic separation, following the manufacturer's protocols. Cells [multiplicity of infection (MOI) = 1.0 $TCID_{50}$ per cell] were infected by centrifugal enhancement (1000*g*, 30 min, room temperature) followed by incubation at 37°C/5% CO_2 for 3 hours. Infected cells were then washed three times in 1× PBS and cultured at 7.5×10^5 cells/ml in serum-low media (XVIVO-15) or RPMI 1640 (ATCC) supplemented with 1% heat-inactivated human serum (Millipore Sigma). Where indicated, mCherry-positive cells were sorted 1 dpi using fluorescence-activated cell sorting (FACS; FACSMelody, BD Biosciences). At 7 dpi, a portion of each infected cell population was cultured in reactivation media [RPMI 1640, containing 10% FBS, with macrophage colony-stimulating factor (10 ng/ml) or maintained under conditions favoring latency (X-VIVO15)].

Pharmacological inhibitors of Src (PP2), MEK (selumetinib), ERK1/2 (SCH772984), or EphA2 (dasatinib) were added, where indicated, at the concentrations specified in the results and/or figure legends. Latent and reactivated cultures were distinguished and quantified by ELDA [(*76*), http://bioinf.wehi.edu.au/software/elda/] on naïve NuFF-1 cells, as described in detail elsewhere (*10*, *16*). Cell viability in the presence of each inhibitor was assessed by live/dead discrimination using trypan blue.

THP-1 monocytic cells were infected (MOI = 1.0 $TCID_{50}$ per cell) at a density of 5.0×10^5 cells/ml by centrifugal enhancement (1000*g* for 30 min, room temperature) in serum-low media (XVIVO-15; Lonza) and then incubated for an additional 60 min at 37°C and 5% CO_2. Viral inoculum was removed, and cells were washed three times with 1× PBS and replated in XVIVO-15 for the duration of the assay, as indicated in the results and/or figure legends.

Protein and RNA analyses

For all immunoblot assays, cells were lysed in radioimmunoprecipitation assay (RIPA) buffer [1% NP-40, 1% sodium deoxycholate, 0.1% SDS, 0.15 M NaCl, 0.01 M $NaPO_4$ (pH 7.2), and 2 mM EDTA] on ice for 1 hour, vortexing every 15 min. Total protein concentrations were quantified by Bradford assay using Protein Assay Dye Reagent Concentrate (Bio-Rad). Samples were denatured at 95°C for 10 min, except for those samples used to detect US28, which were denatured for 10 min at 42°C. Equal amounts of protein per sample were separated by SDS–polyacrylamide gel electrophoresis, and proteins were detected using the following antibodies (table S3): streptavidin–horseradish peroxidase (HRP, Thermo Fisher Scientific), anti-FLAG clone M2 (Millipore Sigma, 1:7500), anti-HA clone 3F10 (Millipore Sigma, 1:1000), anti–phospho-Fos (Ser^{32}) [Cell Signaling Technology (CST), 1:1000], anti–c-Fos (CST, 1:1000), anti–phospho-p44/42 MAPK (ERK1/2; Thr^{202}/Tyr^{204}) (CST, 1:1000), anti-p44/42 MAPK (ERK1/2) (CST, 1:1000), anti–phospho-Src (Tyr^{527}) (CST, 1:1000), anti–phospho-Src (Tyr^{416}) (CST, 1:1000), anti-Src (CST, 1:1000), anti–phospho-MEK1/2 (CST, 1:1000), anti-MEK1/2 (CST, 1:1000), anti–phospho-EphA2 (Ser^{897}) (CST, 1:1000), anti-EphA2 (CST, 1:1000), anti-CMV IE1 [clone 1B12, 1:100, (*77*)], anti–β-actin peroxidase (Millipore Sigma, 1:20,000), and goat anti-mouse, goat anti-rat, and goat anti-rabbit HRP secondary antibodies (all from Jackson ImmunoResearch Labs; 1:10,000). Where indicated, protein expression was quantified by densitometry using ImageJ (*78*).

For co-IP assays of US28 and EphA2, NuFF-1 or $CD14^+$ cells were infected with TB40/E*mCherry*-US28-3xF (MOI = 1.0 $TCID_{50}$ per cell) and harvested as indicated in the results and/or figure legends. Cells were lysed in IP buffer [150 mM NaCl, 25 mM tris (pH 7.4), 10 mM MgCl, 2 mM EDTA, and 1% Triton X-100], supplemented with Complete Protease Inhibitor Cocktail (Millipore Sigma) on ice for 2 hours. Samples were then centrifuged at 12,000*g* for 10 min at 4°C, and an aliquot of $^1/_{20}$ of the total volume was taken for an input control. The indicated protein was precipitated with 5 μl of antibody (anti-FLAG M2, Millipore Sigma; anti-EphA2, CST; rabbit IgG, Millipore Sigma; and mouse IgG, CST), with protein A beads overnight at 4°C with rotation. Beads were then washed four times in IP wash buffer [25 mM tris (pH 7.4), 10 mM MgCl, 2 mM EDTA, and 0.1% Triton X-100] at 4°C, and washes were retained for analysis. Beads, input, and washes were then denatured at 42°C for 10 min. All samples were then immunoblotted as detailed above.

For immunofluorescence assays (IFAs), 2×10^5 NuFF-1 cells were grown on 22 × 22 mm coverslips and infected (MOI = 0.01 $TCID_{50}$ per cell). At 72 hpi, cells were fixed, permeabilized, and stained, as described elsewhere [e.g., (*71*)]. The following antibodies were used, as indicated in the results and/or figure legends: anti-HA (Millipore Sigma, 1:1000) and Alexa 488–conjugated anti-rat (Abcam, 1:1000). Nuclei were visualized with 4′-6′-diamidino-2-phenylindole. Coverslips were mounted onto slides with SlowFade Antifade reagent (Thermo Fisher Scientific), and images were collected using a Leica TCS-SP8-AOBS inverted confocal microscope using Leica Application Suite X (LAS X) Software, version 3.5.5 (Leica Microsystems).

Total RNA was collected, and RNA was extracted using the High Pure RNA Isolation kit (Roche) according to the manufacturer's instructions. cDNA was generated from 1.0 μg of RNA using TaqMan reverse transcription reagents and random hexamer primers (Thermo Fisher Scientific). Equal volumes of cDNA were used for quantitative PCR using primers for either viral *UL123* or cellular *GAPDH* (*glyceraldehyde-3-phosphate dehydrogenase*) (table S4), and transcript abundance was calculated using a standard curve using 10-fold serial dilutions of TB40/E*mCherry*-BAC standard that also contains GAPDH sequence (*16*). Each primer set had a similar amplification efficiency and linear range of detection for the BAC-standard (linear between 10^9 and 10^4 copies; $R^2 > 0.95$ for all experiments). Samples were analyzed in triplicate using a 96-well-format CFX Connect Real-Time PCR instrument (Bio-Rad).

Global kinome analysis

THP-1-pSLIK-hygro and THP-1-pSLIK-US28-3xF were cultured in X-VIVO15 media (Lonza) at 5×10^5 cells/ml and treated with DOX

(1.0 μg/ml). At 2 and 6 hours after DOX treatment, 3×10^7 cells were harvested, washed three times in 1× PBS, and frozen at −80°C. Protein samples were subjected to multiplexed kinase inhibitor beads (MIBS) enrichment, as previously described (*23*). Briefly, cell pellets were lysed [50 mM Hepes (pH 7.5), 150 mM NaCl, 0.5% Triton X-100, 1.0 mM EDTA, 1.0 mM EGTA, 10 mM NaF, 2.5 mM $NaV0_4$ supplemented with Complete Protease Inhibitor Cocktail (Millipore Sigma), and Phosphatase Inhibitor Cocktails 2 and 3 (both from Millipore Sigma)], sonicated (35% power, 3 × 1-s pulses), clarified by centrifugation (14,000*g*, 10 min), and filtered with 0.2-μm surfactant-free cellulose acetate membrane filters. Protein concentrations were determined by Bradford assay, and the salt concentration was adjusted to 1 M NaCl. Poly-Prep chromatography columns (Bio-Rad) were loaded with MIBS resin, consisting of equal volumes of the broad-spectrum type I kinase inhibitors PP58, purvalanol B, VI16832, and UNC21474, and then equilibrated with high-salt wash buffer [50 mM Hepes (pH 7.5), 1.0 M NaCl, 0.5% Triton X-100, 1.0 mM EDTA, and 1.0 mM EGTA] using gravity flow. Lysates were then passed over equilibrated columns by gravity flow. Columns were stringently washed first with high-salt buffer, then low-salt buffer [50 mM Hepes (pH 7.5), 150 mM NaCl, 0.5% Triton X-100, 1.0 mM EDTA, and 1.0 mM EGTA], and, lastly, SDS wash buffer [50 mM Hepes (pH 7.5), 150 mM NaCl, 0.5% Triton X-100, 0.1% SDS, 1.0 mM EDTA, and 1.0 mM EGTA]. Proteins were eluted from the column by boiling in elution buffer [100 mM tris-HCl (pH 6.8), 0.5% SDS, and 1% β-mercaptoethanol]. Eluates were reduced (5 mM DL-dithiothreitol, 30 min, 60°C), alkylated (20 mM iodoacetamide, 30 min, room temperature), and concentrated (Amicon Ultra-4 Centrifugal Filter Units; Millipore Sigma). Protein was extracted with chloroform-methanol precipitation and digested overnight with sequencing grade porcine trypsin (Promega). Peptides were then extracted with three ethyl acetate washes and desalted using Pierce C-18 spin columns (Thermo Fisher Scientific), according to the manufacturer's protocol.

Affinity purification MS

NuFF-1 cells (1×10^7 cells per condition) were TB40/E*mCherry*–, TB40/E*mCherry*-US28-BirA-HA–, or mock-infected at a multiplicity of 1.0 $TCID_{50}$ per cell. Infected and uninfected control cells were treated with or without biotin (50 μM final concentration) 18 hours before harvest. Cells were harvested at 48 hpi, washed three times with 1× PBS, and then resuspended in 1.0 ml of ice-cold RIPA lysis buffer [50 mM, tris (pH 7.4), 150 mM NaCl, 1% NP-40, 0.25% Na deoxycholate, 1.0 mM EDTA, and 2 M Urea]. Cells were allowed to swell on ice for 15 min and sonicated (three pulses, 30% output). Cellular debris was removed by centrifugation, and biotinylated proteins were isolated from the clarified lysate by binding to Dynabeads MyOne Streptavidin T1 (Thermo Fisher Scientific) for 3 hours at 4°C. Using a DynaMag-2 Magnet (Thermo Fisher Scientific), beads were washed three times in RIPA lysis buffer and then three times with 50 mM ammonium bicarbonate (pH 8.0). Cells were resuspended in a final volume of 100 μl of 50 mM ammonium bicarbonate (pH 8.0) for tandem MS (MS/MS) analysis. Aliquots of clarified lysate (50 μl) and aliquots of resuspended beads (2 μl) were reserved for immunoblot analysis.

Protein samples were subjected to on-bead trypsin digestion, as previously described (*79*). After the last wash step, 50 μl of 50 mM ammonium bicarbonate (pH 8.0) containing 1 μg of trypsin (Promega) was added to beads overnight at 37°C with shaking. The next day, 500 ng of trypsin was added and then incubated for an additional 3 hours at 37°C with shaking. The clarified supernatants were transferred, and the beads were washed twice with 50 μl of liquid chromatography–MS (LC/MS) grade water. The washes were then combined with the original supernatant and then acidified to 2% formic acid. Peptides were desalted with Pierce Peptide Desalting Spin Columns (Thermo Fisher Scientific) and dried via vacuum centrifugation. Peptide samples were stored at −80°C until further analysis.

Liquid chromatography–tandem MS

Peptide samples from both the MIB-MS and AP-MS sample sets were analyzed by LC-MS/MS using an Easy nLC 1200 coupled to a QExactive HF mass spectrometer (Thermo Fisher Scientific). Samples were injected onto an EASY-Spray PepMap C18 column (75 μm inner diameter × 25 cm, 2 μm particle size; Thermo Fisher Scientific) and separated over a 120-min method. The gradient for separation consisted of 5 to 40% mobile phase B at a 250 nl/min flow rate, where mobile phase A was 0.1% formic acid in water, and mobile phase B consisted of 0.1% formic acid in 80% acetonitrile. The QExactive HF was operated in data-dependent mode, where the 15 most intense precursors were selected for subsequent fragmentation. Resolution for the precursor scan (mass/charge ratio, 350 to 1600) was set to 120,000 with a target value of 3×10^6 ions. MS/MS scan resolution was set to 15,000 with a target value of 5×10^4 ions, 60 ms maximum injection time. The normalized collision energy was set to 27% for high collision dissociation. Dynamic exclusion was set to 30 s, peptide match was set to preferred, and precursors with unknown charge or a charge state of 1 and ≥ 7 were excluded.

MS data analyses

Raw data were processed using the MaxQuant software suite (version 1.6.12.0) for identification and label-free quantitation (LFQ) (*80*). Data were searched against a UniProt Human database (containing 20,350 sequences, downloaded February 2020; taxonomy ID, 9606; proteome ID, UP000005640) and a UniProt CMV TB40/E database (containing 164 sequences, downloaded April 2016; taxonomy ID, 10359; proteome ID, UP000143167) using the integrated Andromeda search engine (*81*). A maximum of two missed tryptic cleavages were allowed. The variable modification specified was oxidation of methionine and N-terminal acetylation. LFQ was enabled. Results were filtered to 1% FDR at the unique peptide level and grouped into proteins within MaxQuant. Match between runs was enabled.

For kinome analysis, carbamidomethylation of cysteine was set as a fixed modification, and all other parameters were the same as above. Kinases were parsed, and global normalization was applied. Argonaut (*82*) was used for further processing. Only proteins with >1 unique+razor peptide were used for LFQ analysis. Proteins with >50% missing values were removed, and missing values were replaced from normal distribution. Log_2 fold change ratios (2 hpi_control and 6 hpi_control) were calculated using the averaged log_2 LFQ intensities and proteins, with $|log_2 \text{ fold change}| \geq 1$ considered significant. Student's *t* test was performed, and $P < 0.05$ was considered significant.

For AP-MS analysis, results were searched against the CRAPome database (*29*), and proteins with CRAPome frequency > 30% were removed. Perseus (*83*) was used for further processing. Only proteins with >1 unique+razor peptide were used for LFQ analysis. Proteins with >50% missing values were removed, and missing values were replaced from normal distribution. Log_2 fold change ratios (48 hpi_all

controls) were calculated using the averaged $\log_2$ LFQ intensities. Student's *t* test was performed, and *P* values and permutation-based FDR-corrected *q* values were calculated (*84*). Proteins were considered US28 interactors if the CRAPome frequency is <30%, FDR-corrected *q* value < 0.05, and $\log_2$ fold change ratio > 1.

Viral growth assays

Multistep growth assays were performed by infecting (MOI = 0.01 $TCID_{50}$ per cell) naïve NuFF-1 cells or those stably transduced with lentiviruses expressing nontargeting control (NTC)–shRNA, EphA2-shRNA#1, or EphA2-shRNA#2. Supernatants were collected over a 16-day time course of infection and stored at −80°C until processing. At 16 dpi, infected cells were washed three times with 1× PBS and collected in media to evaluate cell-associated viral titers. To this end, cells were subjected to three freeze-thaw cycles, after which cellular debris was removed by centrifugation and the clarified supernatant was collected. Cell-free and cell-associated virus was quantified by $TCID_{50}$ assay.

Clinical data analyses

A retrospective cohort analysis was conducted in December 2021, using the multiple health system data analytics and research platform, Explorys (IBM Explorys Cohort Discovery, Watson Health; https://ibm.com/products/explorys-ehr-data-analysis-tools), which provides aggregated, de-identified EHR data from more than 53 million unique patients throughout the United States. Longitudinal records for unique patients are generated by standardizing the different EHR data using the single set of Unified Medical Language System ontologies. Patient data are de-identified; therefore, ethical review and informed consent is waived, although to further protect patient confidentiality, the system rounds patient counts per search term to the nearest 10. Data were analyzed from the EHRs from more than 53 million unique patients, and data from patients of all ages, sexes, and ethnicities were included in our study. Information on age, sex, and ethnicity was not collected as part of our study. The initial search term used was "dasatinib," and the resulting 3230 patient records were then cross-referenced for diagnosis of disease and/or infection for the following herpesviruses: HSV-1, HSV-2, VZV, EBV, CMV, HHV-6, HHV-7, or KSHV (HHV-8). ORs and 95% CIs were determined by Fisher's exact test (MedCalc Software; https://medcalc.org/calc/odds_ratio.php). Statistical tests were adjusted for multiple testing using Benjamini-Hochberg FDR correction, and an FDR-corrected $P < 0.05$ was used as the threshold for statistical significance (*85*). Use of Explorys at the Cleveland Clinic is approved under Institutional Review Board no. 19-504.

Statistical analyses

Experimental data were analyzed by GraphPad Prism (version 9.1.0) software (GraphPad Software LLC) and Microsoft Excel (version 16.59). The statistical details for each experiment are provided in the respective figure legends. The statistical analyses for the proteomics experiments are detailed above. A minimum of three biological replicates ($n = 3$) were performed for all experiments. Protein data, including immunoblots and IFAs, are shown as representative biological replicates, as indicated in the respective figure legends. Representative biological replicates are shown for the $TCID_{50}$ data (fig. S5, B and C), each of which had three technical replicates, as indicated in the figure legend. For the ELDA data, three biological replicates were performed, each of which contained three technical replicates. Each data point on the graphs (denoted by circles) represents the mean of the three technical replicates. Error bars indicate the SD of the three biological replicates. Statistical significance for all data was calculated by one-way or two-way analysis of variance, as indicated in the figure legends, with Tukey's test for multiple comparisons. In all cases, $P < 0.05$ was considered significant. Analysis of the Explorys data is described above in detail.

SUPPLEMENTARY MATERIALS

Supplementary material for this article is available at https://science.org/doi/10.1126/sciadv.add1168

View/request a protocol for this paper from *Bio-protocol*.

REFERENCES AND NOTES

1. E. Forte, Z. Zhang, E. B. Thorp, M. Hummel, Cytomegalovirus latency and reactivation: An intricate interplay with the host immune response. *Front. Cell. Infect. Microbiol.* **10**, 130 (2020).
2. A. Meesing, R. R. Razonable, New developments in the management of cytomegalovirus infection after transplantation. *Drugs* **78**, 1085–1103 (2018).
3. D. E. Johnson, Src family kinases and the MEK/ERK pathway in the regulation of myeloid differentiation and myeloid leukemogenesis. *Adv. Enzyme Regul.* **48**, 98–112 (2008).
4. H. Miao, B. R. Wei, D. M. Peehl, Q. Li, T. Alexandrou, J. R. Schelling, J. S. Rhim, J. R. Sedor, E. Burnett, B. Wang, Activation of EphA receptor tyrosine kinase inhibits the Ras/MAPK pathway. *Nat. Cell Biol.* **3**, 527–530 (2001).
5. M. G. Coulthard, M. Morgan, T. M. Woodruff, T. V. Arumugam, S. M. Taylor, T. C. Carpenter, M. Lackmann, A. W. Boyd, Eph/Ephrin signaling in injury and inflammation. *Am. J. Pathol.* **181**, 1493–1503 (2012).
6. E. G. Elder, B. A. Krishna, E. Poole, M. Perera, J. Sinclair, Regulation of host and viral promoters during human cytomegalovirus latency via US28 and CTCF. *J. Gen. Virol.* **102**, 001609 (2021).
7. E. G. Elder, B. A. Krishna, J. Williamson, E. Y. Lim, E. Poole, G. X. Sedikides, M. Wills, C. M. O'Connor, P. J. Lehner, J. Sinclair, Interferon-responsive genes are targeted during the establishment of human cytomegalovirus latency. *MBio* **10**, e02574–e02519 (2019).
8. M. S. Humby, C. M. O'Connor, Human cytomegalovirus US28 is important for latent infection of hematopoietic progenitor cells. *J. Virol.* **90**, 2959–2970 (2015).
9. B. A. Krishna, K. Spiess, E. L. Poole, B. Lau, S. Voigt, T. N. Kledal, M. M. Rosenkilde, J. H. Sinclair, Targeting the latent cytomegalovirus reservoir with an antiviral fusion toxin protein. *Nat. Commun.* **8**, 14321 (2017).
10. B. A. Krishna, M. S. Humby, W. E. Miller, C. M. O'Connor, Human cytomegalovirus G protein-coupled receptor US28 promotes latency by attenuating c-fos. *Proc. Natl. Acad. Sci. U.S.A.* **116**, 1755–1764 (2019).
11. B. A. Krishna, E. L. Poole, S. E. Jackson, M. J. Smit, M. R. Wills, J. H. Sinclair, Latency-associated expression of human cytomegalovirus US28 attenuates cell signaling pathways to maintain latent infection. *MBio* **8**, e01754–e01717 (2017).
12. B. A. Krishna, A. B. Wass, R. Sridharan, C. M. O'Connor, The requirement for US28 during cytomegalovirus latency is independent of US27 and US29 gene expression. *Front. Cell. Infect. Microbiol.* **10**, 186 (2020).
13. S.-E. Wu, W. E. Miller, The HCMV US28 vGPCR induces potent Gαq/PLC-β signaling in monocytes leading to increased adhesion to endothelial cells. *Virology* **497**, 233–243 (2016).
14. D. Zhu, C. Pan, J. Sheng, H. Liang, Z. Bian, Y. Liu, P. Trang, J. Wu, F. Liu, C.-Y. Zhang, K. Zen, Human cytomegalovirus reprogrammes haematopoietic progenitor cells into immunosuppressive monocytes to achieve latency. *Nat. Microbiol.* **3**, 503–513 (2018).
15. A. L. Dooley, C. M. O'Connor, Regulation of the MIE locus during HCMV latency and reactivation. *Pathogens* **9**, 869 (2020).
16. B. A. Krishna, A. B. Wass, C. M. O'Connor, Activator protein-1 transactivation of the major immediate early locus is a determinant of cytomegalovirus reactivation from latency. *Proc. Natl. Acad. Sci. U.S.A.* **117**, 20860–20867 (2020).
17. K. Okazaki, N. Sagata, The Mos/MAP kinase pathway stabilizes c-Fos by phosphorylation and augments its transforming activity in NIH 3T3 cells. *EMBO J.* **14**, 5048–5059 (1995).
18. B. A. Krishna, W. E. Miller, C. M. O'Connor, US28: HCMV's Swiss army knife. *Viruses* **10**, 445 (2018).
19. M. B. Reeves, Cell signaling and cytomegalovirus reactivation: What do Src family kinases have to do with it? *Biochem. Soc. Trans.* **48**, 667–675 (2020).
20. S. Fujioka, J. Niu, C. Schmidt, G. M. Sclabas, B. Peng, T. Uwagawa, Z. Li, D. B. Evans, J. L. Abbruzzese, P. J. Chiao, NF-κB and AP-1 connection: Mechanism of NF-κB-dependent regulation of AP-1 activity. *Mol. Cell. Biol.* **24**, 7806–7819 (2004).
21. E. Toton, N. Lisiak, B. Rubis, J. Budzianowski, P. Gruber, J. Hofmann, M. Rybczynska, The tetramethoxyflavone zapotin selectively activates protein kinase C epsilon, leading to its

down-modulation accompanied by Bcl-2, c-Jun and c-Fos decrease. *Eur. J. Pharmacol.* **682**, 21–28 (2012).
22. W. E. Miller, W. A. Zagorski, J. D. Brenneman, D. Avery, J. L. C. Miller, C. M. O'Connor, US28 is a potent activator of phospholipase C during HCMV infection of clinically relevant target cells. *PLOS ONE* **7**, e50524 (2012).
23. K. C. Arend, E. M. Lenarcic, H. A. Vincent, N. Rashid, E. Lazear, I. M. McDonald, T. S. Gilbert, M. P. East, L. E. Herring, G. L. Johnson, L. M. Graves, N. J. Moorman, Kinome profiling identifies druggable targets for novel human cytomegalovirus (HCMV) antivirals. *Mol. Cell. Proteomics* **16**, S263–S276 (2017).
24. J. S. Zawistowski, L. M. Graves, G. L. Johnson, Assessing adaptation of the cancer kinome in response to targeted therapies. *Biochem. Soc. Trans.* **42**, 765–769 (2014).
25. M. Macrae, R. M. Neve, P. Rodriguez-Viciana, C. Haqq, J. Yeh, C. Chen, J. W. Gray, F. McCormick, A conditional feedback loop regulates Ras activity through EphA2. *Cancer Cell* **8**, 111–118 (2005).
26. Q. Chang, C. Jorgensen, T. Pawson, D. W. Hedley, Effects of dasatinib on EphA2 receptor tyrosine kinase activity and downstream signalling in pancreatic cancer. *Br. J. Cancer* **99**, 1074–1082 (2008).
27. D. P. Prestes, E. Arbona, A. Nevett-Fernandez, A. E. Woolley, V. T. Ho, S. Koo, L. R. Baden, J. Koreth, S. P. Hammond, N. C. Issa, F. M. Marty, Dasatinib use and risk of cytomegalovirus reactivation after allogeneic hematopoietic-cell transplantation. *Clin. Infect. Dis.* **65**, 510–513 (2017).
28. K. J. Roux, D. I. Kim, M. Raida, B. Burke, A promiscuous biotin ligase fusion protein identifies proximal and interacting proteins in mammalian cells. *J. Cell Biol.* **196**, 801–810 (2012).
29. D. Mellacheruvu, Z. Wright, A. L. Couzens, J. P. Lambert, N. A. St-Denis, T. Li, Y. V. Miteva, S. Hauri, M. E. Sardiu, T. Y. Low, V. A. Halim, R. D. Bagshaw, N. C. Hubner, A. Al-Hakim, A. Bouchard, D. Faubert, D. Fermin, W. H. Dunham, M. Goudreault, Z. Y. Lin, B. G. Badillo, T. Pawson, D. Durocher, B. Coulombe, R. Aebersold, G. Superti-Furga, J. Colinge, A. J. Heck, H. Choi, M. Gstaiger, S. Mohammed, I. M. Cristea, K. L. Bennett, M. P. Washburn, B. Raught, R. M. Ewing, A. C. Gingras, A. I. Nesvizhskii, The CRAPome: A contaminant repository for affinity purification-mass spectrometry data. *Nat. Methods* **10**, 730–736 (2013).
30. L.-F. Yee, P. L. Lin, M. F. Stinski, Ectopic expression of HCMV IE72 and IE86 proteins is sufficient to induce early gene expression but not production of infectious virus in undifferentiated promonocytic THP-1 cells. *Virology* **363**, 174–188 (2007).
31. Y. Fang, L. Zhong, M. Lin, X. Zhou, H. Jing, M. Ying, P. Luo, B. Yang, Q. He, MEK/ERK dependent activation of STAT1 mediates dasatinib-induced differentiation of acute myeloid leukemia. *PLOS ONE* **8**, e66915 (2013).
32. L. M. Packer, S. Rana, R. Hayward, T. O'Hare, C. A. Eide, A. Rebocho, S. Heidorn, M. S. Zabriskie, I. Niculescu-Duvaz, B. J. Druker, C. Springer, R. Marais, Nilotinib and MEK inhibitors induce synthetic lethality through paradoxical activation of RAF in drug-resistant chronic myeloid leukemia. *Cancer Cell* **20**, 715–727 (2011).
33. E. C. W. de Boer, J. M. van Gils, M. J. van Gils, Ephrin-Eph signaling usage by a variety of viruses. *Pharmacol. Res.* **159**, 105038 (2020).
34. T. P. Light, D. Brun, P. Guardado-Calvo, R. Pederzoli, A. Haouz, F. Neipel, F. A. Rey, K. Hristova, M. Backovic, Human herpesvirus 8 molecular mimicry of ephrin ligands facilitates cell entry and triggers EphA2 signaling. *PLoS Biol.* **19**, e3001392 (2021).
35. C. Su, L. Wu, Y. Chai, J. Qi, S. Tan, G. F. Gao, H. Song, J. Yan, Molecular basis of EphA2 recognition by gHgL from gammaherpesviruses. *Nat. Commun.* **11**, 5964 (2020).
36. N. Wallaschek, S. Reuter, S. Silkenat, K. Wolf, C. Niklas, Ö. Kayisoglu, C. Aguilar, A. Wiegering, C.-T. Germer, S. Kircher, A. Rosenwald, C. Shannon-Lowe, S. Bartfeld, Ephrin receptor A2, the epithelial receptor for Epstein-Barr virus entry, is not available for efficient infection in human gastric organoids. *PLOS Pathog.* **17**, e1009210 (2021).
37. N. J. Pyne, C. M. Waters, J. S. Long, N. A. Moughal, G. Tigyi, S. Pyne, Receptor tyrosine kinase-G-protein coupled receptor complex signaling in mammalian cells. *Adv. Enzyme Regul.* **47**, 271–280 (2007).
38. L. E. Kilpatrick, S. J. Hill, Transactivation of G protein-coupled receptors (GPCRs) and receptor tyrosine kinases (RTKs): Recent insights using luminescence and fluorescence technologies. *Curr. Opin. Endocr. Metab. Res.* **16**, 102–112 (2021).
39. N. J. Smith, L. M. Luttrell, Signal switching, crosstalk, and arrestin scaffolds: Novel G protein-coupled receptor signaling in cardiovascular disease. *Hypertension* **48**, 173–179 (2006).
40. M. P. Stropes, O. D. Schneider, W. A. Zagorski, J. L. C. Miller, W. E. Miller, The carboxy-terminal tail of human cytomegalovirus (HCMV) US28 regulates both chemokine-independent and chemokine-dependent signaling in HCMV-infected cells. *J. Virol.* **83**, 10016–10027 (2009).
41. M. P. M. Stropes, W. E. Miller, Functional analysis of human cytomegalovirus pUS28 mutants in infected cells. *J. Gen. Virol.* **89**, 97–105 (2008).
42. W. Dunn, C. Chou, H. Li, R. Hai, D. Patterson, V. Stolc, H. Zhu, F. Liu, Functional profiling of a human cytomegalovirus genome. *Proc. Natl. Acad. Sci. U.S.A.* **100**, 14223–14228 (2003).
43. J. Vieira, T. J. Schall, L. Corey, A. P. Geballe, Functional analysis of the human cytomegalovirus US28 gene by insertion mutagenesis with the green fluorescent protein gene. *J. Virol.* **72**, 8158–8165 (1998).
44. D. Yu, M. C. Silva, T. Shenk, Functional map of human cytomegalovirus AD169 defined by global mutational analysis. *Proc. Natl. Acad. Sci. U.S.A.* **100**, 12396–12401 (2003).
45. H. A. Torres, R. F. Chemaly, Viral infection or reactivation in patients during treatment with dasatinib: A call for screening? *Leuk. Lymphoma* **48**, 2308–2309 (2007).
46. T.-M. Chuang, C.-M. Hsu, P.-I. Liang, H.-H. Hsiao, Cytomegalovirus colitis with presentation of hemorrhagic colitis in chronic myeloid leukemia during dasatinib therapy. *J. Formos. Med. Assoc.* **120**, 1155–1157 (2021).
47. A. Nakaya, Y. Azuma, S. Fujita, A. Satake, T. Nakanishi, Y. Tsubokura, A. Konishi, M. Hotta, H. Yoshimura, K. Ishii, T. Ito, S. Nomura, Dasatinib-induced hemorrhagic colitis complicated with cytomegalovirus infection. *Hematol. Rep.* **9**, 7415 (2017).
48. M. A. Yassin, A. J. Nashwan, A. T. Soliman, A. Yousif, A. Moustafa, A. AlBattah, S. F. Mohamed, D. S. Mudawi, S. Elkourashy, D.-R. Asaari, H.-L. G. Gutierrez, M. Almusharaf, R. M. Hussein, A. H. Moustafa, H. E. Derhoubi, S. Boukhris, S. Kohla, N. AlDewik, Cytomegalovirus-induced hemorrhagic colitis in a patient with chronic myeloid leukemia (chronic phase) on dasatinib as an upfront therapy. *Clin. Med. Insights Case Rep.* **8**, 77–81 (2015).
49. J. K. Choi, S. Y. Cho, S. M. Choi, G. H. Kim, S. E. Lee, S. Lee, D. W. Kim, D. G. Lee, Cytomegalovirus colitis during dasatinib treatment for patients with hematologic malignancy: Case series and literature review. *Infect. Chemother.* **50**, 153–159 (2018).
50. I. Aldoss, K. Gaal, M. M. Al Malki, H. Ali, R. Nakamura, S. J. Forman, V. Pullarkat, Dasatinib-induced colitis after allogeneic stem cell transplantation for philadelphia chromosome-positive acute lymphoblastic leukemia. *Biol. Blood Marrow Transplant* **22**, 1900–1903 (2016).
51. F. Davalos, B. Chaucer, W. Zafar, S. Salman, J. Nfonoyim, Dasatinib-induced CMV hepatitis in an immunocompetent patient: A rare complication of a common drug. *Transl. Oncol.* **9**, 248–250 (2016).
52. S. J. Blake, A. Bruce Lyons, C. K. Fraser, J. D. Hayball, T. P. Hughes, Dasatinib suppresses in vitro natural killer cell cytotoxicity. *Blood* **111**, 4415–4416 (2008).
53. F. Fei, Y. Yu, A. Schmitt, M. T. Rojewski, B. Chen, M. Götz, H. Döhner, D. Bunjes, M. Schmitt, Dasatinib inhibits the proliferation and function of $CD4^+CD25^+$ regulatory T cells. *Br. J. Haematol.* **144**, 195–205 (2009).
54. F. Fei, Y. Yu, A. Schmitt, M. T. Rojewski, B. Chen, J. Greiner, M. Götz, P. Guillaume, H. Döhner, D. Bunjes, M. Schmitt, Dasatinib exerts an immunosuppressive effect on $CD8^+$ T cells specific for viral and leukemia antigens. *Exp. Hematol.* **36**, 1297–1308 (2008).
55. A. E. Schade, G. L. Schieven, R. Townsend, A. M. Jankowska, V. Susulic, R. Zhang, H. Szpurka, J. P. Maciejewski, Dasatinib, a small-molecule protein tyrosine kinase inhibitor, inhibits T-cell activation and proliferation. *Blood* **111**, 1366–1377 (2008).
56. R. Weichsel, C. Dix, L. Wooldridge, M. Clement, A. Fenton-May, A. K. Sewell, J. Zezula, E. Greiner, E. Gostick, D. A. Price, H. Einsele, R. Seggewiss, Profound inhibition of antigen-specific T-cell effector functions by dasatinib. *Clin. Cancer Res.* **14**, 2484–2491 (2008).
57. C. Sillaber, H. Herrmann, K. Bennett, U. Rix, C. Baumgartner, A. Bohm, S. Herndlhofer, E. Tschachler, G. Superti-Furga, U. Jäger, P. Valent, Immunosuppression and atypical infections in CML patients treated with dasatinib at 140 mg daily. *Eur. J. Clin. Invest.* **39**, 1098–1109 (2009).
58. D. H. Kim, S. Kamel-Reid, H. Chang, R. Sutherland, C. W. Jung, H.-J. Kim, J.-J. Lee, J. H. Lipton, Natural killer or natural killer/T cell lineage large granular lymphocytosis associated with dasatinib therapy for Philadelphia chromosome positive leukemia. *Haematologica* **94**, 135–139 (2009).
59. A. Kreutzman, V. Juvonen, V. Kairisto, M. Ekblom, L. Stenke, R. Seggewiss, K. Porkka, S. Mustjoki, Mono/oligoclonal T and NK cells are common in chronic myeloid leukemia patients at diagnosis and expand during dasatinib therapy. *Blood* **116**, 772–782 (2010).
60. S. Mustjoki, M. Ekblom, T. P. Arstila, I. Dybedal, P. K. Epling-Burnette, F. Guilhot, H. Hjorth-Hansen, M. Höglund, P. Kovanen, T. Laurinolli, J. Liesveld, R. Paquette, J. Pinilla-Ibarz, A. Rauhala, N. Shah, B. Simonsson, M. Sinisalo, J. L. Steegmann, L. Stenke, K. Porkka, Clonal expansion of T/NK-cells during tyrosine kinase inhibitor dasatinib therapy. *Leukemia* **23**, 1398–1405 (2009).
61. A. Kreutzman, K. Ladell, C. Koechel, E. Gostick, M. Ekblom, L. Stenke, T. Melo, H. Einsele, K. Porkka, D. A. Price, S. Mustjoki, R. Seggewiss, Expansion of highly differentiated $CD8^+$ T-cells or NK-cells in patients treated with dasatinib is associated with cytomegalovirus reactivation. *Leukemia* **25**, 1587–1597 (2011).
62. H. Tanaka, S. Nakashima, M. Usuda, Rapid and sustained increase of large granular lymphocytes and rare cytomegalovirus reactivation during dasatinib treatment in chronic myelogenous leukemia patients. *Int. J. Hematol.* **96**, 308–319 (2012).
63. C. Hutterer, S. K. Wandinger, S. Wagner, R. Müller, T. Stamminger, I. Zeitträger, K. Godl, R. Baumgartner, S. Strobl, M. Marschall, Profiling of the kinome of cytomegalovirus-infected cells reveals the functional importance of host kinases Aurora A, ABL and AMPK. *Antiviral. Res.* **99**, 139–148 (2013).

64. R. Buettner, T. Mesa, A. Vultur, F. Lee, R. Jove, Inhibition of Src family kinases with dasatinib blocks migration and invasion of human melanoma cells. *Mol. Cancer Res.* **6**, 1766–1774 (2008).
65. D. Caccia, F. Micciche, G. Cassinelli, P. Mondellini, P. Casalini, I. Bongarzone, Dasatinib reduces FAK phosphorylation increasing the effects of RPI-1 inhibition in a RET/PTC1-expressing cell line. *Mol. Cancer* **9**, 278 (2010).
66. T. Chen, C. Wang, Q. Liu, Q. Meng, H. Sun, X. Huo, P. Sun, J. Peng, Z. Liu, X. Yang, K. Liu, Dasatinib reverses the multidrug resistance of breast cancer MCF-7 cells to doxorubicin by downregulating P-gp expression via inhibiting the activation of ERK signaling pathway. *Cancer Biol. Ther.* **16**, 106–114 (2015).
67. M. Higuchi, K. Ishiyama, M. Maruoka, R. Kanamori, A. Takaori-Kondo, N. Watanabe, Paradoxical activation of c-Src as a drug-resistant mechanism. *Cell Rep.* **34**, 108876 (2021).
68. J. Huang, W. Hu, J. Bottsford-Miller, T. Liu, H. D. Han, B. Zand, S. Pradeep, J.-W. Roh, D. Thanapprapasr, H. J. Dalton, C. V. Pecot, R. Rupaimoole, C. Lu, B. Fellman, D. Urbauer, Y. Kang, N. B. Jennings, L. Huang, M. T. Deavers, R. Broaddus, R. L. Coleman, A. K. Sood, Cross-talk between EphA2 and BRaf/CRaf is a key determinant of response to dasatinib. *Clin. Cancer Res.* **20**, 1846–1855 (2014).
69. J. Buehler, E. Carpenter, S. Zeltzer, S. Igarashi, M. Rak, I. Mikell, J. A. Nelson, F. Goodrum, Host signaling and EGR1 transcriptional control of human cytomegalovirus replication and latency. *PLOS Pathog.* **15**, e1008037 (2019).
70. L. B. Crawford, P. Caposio, C. Kreklywich, A. H. Pham, M. H. Hancock, T. A. Jones, P. P. Smith, A. D. Yurochko, J. A. Nelson, D. N. Streblow, Human cytomegalovirus US28 ligand binding activity is required for latency in $CD34^+$ hematopoietic progenitor cells and humanized NSG mice. *MBio* **10**, e01889-19 (2019).
71. C. M. O'Connor, T. Shenk, Human cytomegalovirus pUS27 G protein-coupled receptor homologue is required for efficient spread by the extracellular route but not for direct cell-to-cell spread. *J. Virol.* **85**, 3700–3707 (2011).
72. S. Warming, N. Costantino, D. L. Court, N. A. Jenkins, N. G. Copeland, Simple and highly efficient BAC recombineering using galK selection. *Nucleic Acids Res.* **33**, e36 (2005).
73. B. A. Krishna, A. B. Wass, A. L. Dooley, C. M. O'Connor, CMV-encoded GPCR pUL33 activates CREB and facilitates its recruitment to the MIE locus for efficient viral reactivation. *J. Cell Sci.* **134**, jcs254268 (2021).
74. K.-J. Shin, E. A. Wall, J. R. Zavzavadjian, L. A. Santat, J. Liu, J.-I. Hwang, R. Rebres, T. Roach, W. Seaman, M. I. Simon, I. D. C. Fraser, A single lentiviral vector platform for microRNA-based conditional RNA interference and coordinated transgene expression. *Proc. Natl. Acad. Sci. U.S.A.* **103**, 13759–13764 (2006).
75. S. A. Stewart, D. M. Dykxhoorn, D. Palliser, H. Mizuno, E. Y. Yu, D. S. An, D. M. Sabatini, I. S. Chen, W. C. Hahn, P. A. Sharp, R. A. Weinberg, C. D. Novina, Lentivirus-delivered stable gene silencing by RNAi in primary cells. *RNA* **9**, 493–501 (2003).
76. Y. Hu, G. K. Smyth, ELDA: Extreme limiting dilution analysis for comparing depleted and enriched populations in stem cell and other assays. *J. Immunol. Methods* **347**, 70–78 (2009).
77. H. Zhu, Y. Shen, T. Shenk, Human cytomegalovirus IE1 and IE2 proteins block apoptosis. *J. Virol.* **69**, 7960–7970 (1995).
78. C. A. Schneider, W. S. Rasband, K. W. Eliceiri, NIH Image to ImageJ: 25 years of image analysis. *Nat. Methods* **9**, 671–675 (2012).
79. L. Rank, L. E. Herring, M. Braunstein, Evidence for the mycobacterial Mce4 transporter being a multiprotein complex. *J. Bacteriol.* **203**, e00685-20 (2021).
80. J. Cox, M. Mann, MaxQuant enables high peptide identification rates, individualized p.p.b.-range mass accuracies and proteome-wide protein quantification. *Nat. Biotechnol.* **26**, 1367–1372 (2008).
81. UniProt Consortium, UniProt: The universal protein knowledgebase in 2021. *Nucleic Acids Res.* **49**, D480–D489 (2021).
82. D. R. Brademan, I. J. Miller, N. W. Kwiecien, D. J. Pagliarini, M. S. Westphall, J. J. Coon, E. Shishkova, Argonaut: A web platform for collaborative multi-omic data visualization and exploration. *Patterns* **1**, 100122 (2020).
83. S. Tyanova, T. Temu, P. Sinitcyn, A. Carlson, M. Y. Hein, T. Geiger, M. Mann, J. Cox, The Perseus computational platform for comprehensive analysis of (prote)omics data. *Nat. Methods* **13**, 731–740 (2016).
84. S. Tyanova, J. Cox, Perseus: A bioinformatics platform for integrative analysis of proteomics data in cancer research. *Methods Mol. Biol.* **1711**, 133–148 (2018).
85. Y. Benjamini, Y. Hochberg, Controlling the false discovery rate: A practical and powerful approach to multiple testing. *J. R. Stat. Soc.* **57**, 289–300 (1995).

Acknowledgments: We thank W. Zuercher for assistance with pharmacological inhibitor selection and J. Hockings for helpful discussions regarding pharmacokinetics. We thank A. Prevatte and N. Barker at the UNC Proteomics Core for assistance with proteomics sample preparation. We also thank J. Peterson in the Cleveland Clinic Imaging Core for assistance with confocal microscopy, as well as A. Graham, J. Korecky, and E. Schultz in the Cleveland Clinic Flow Cytometry Core for assistance with cell sorting. Last, we would like to thank E. Murphy, G. Chan, G. Sen, and T. Stappenbeck for helpful discussions. **Funding:** This work was supported by National Institutes of Health Shared Instrumentation grant S10OD019972 (Cleveland Clinic), National Institutes of Health grant P30CA16086 (UNC Lineberger Comprehensive Cancer Center), Case Comprehensive Cancer Center American Cancer Society Internal Research grant RES516032 (C.M.O.), National Institutes of Health grant R01AI153348 (C.M.O.), National Institutes of Health grant R01AI150931 (C.M.O.), American Heart Association and the Hablitzel Family Predoctoral award 20PRE35080060 (A.L.D.), and Cleveland Clinic Research Co-Laboratory award (D.M.R. and C.M.O.). **Author contributions:** Conceptualization: B.A.K., M.N., and C.M.O. Methodology: A.B.W., B.A.K., and C.M.O. Formal analysis: A.B.W., B.A.K., L.E.H., T.S.K.G., M.N., I.J.G., A.L.D., K.H.K., and D.M.R. Investigation: A.B.W., B.A.K., L.E.H., T.S.K.G., M.N., I.J.G., A.L.D., K.H.K., and S.M.M. Resources: A.B.W., B.A.K., M.N., and A.L.D. Supervision: L.E.H., L.M.G., and C.M.O. Writing—original draft: B.A.K. and C.M.O. Writing—review and editing: A.B.W., B.A.K., L.E.H., T.S.K.G., I.J.G., A.L.D., K.H.K., S.M.M., D.M.R., L.M.G., and C.M.O. Visualization: A.B.W., B.A.K., L.E.H., I.J.G., A.L.D., and K.H.K. Funding acquisition: A.L.D., D.M.R., L.M.G., and C.M.O. **Competing interests:** D.M.R. has stock and other ownership interests in Clarified Precision Medicine, has served in a consultant and advisory role for Pharmazam, has received research funding from Novo Nordisk, and has intellectual property related to the detection of liver cancer. L.M.G. is a cofounder of Virokyne LLC. All other authors declare that they have no competing interests. **Data and materials availability:** All data needed to evaluate the conclusions in the paper are present in the paper, the Supplementary Materials, or publicly accessible repositories. The proteomics datasets generated and analyzed during the current study are available in the Proteomics Identification Database (PRIDE) repository under project identifier PXD033391 and are publicly available as of the date of publication. Newly generated viruses and cell lines can be requested from the corresponding author, following institutional guidelines for material transfer agreements.

Submitted 21 May 2022
Accepted 1 September 2022
Published 26 October 2022
10.1126/sciadv.add1168